Journal of Ocean and Wind Energy (ISSN 2310-3604)
Copyright © by The International Society of Offshore and Polar Engineers
Vol. 2, No. 3, August 2015, pp. 176–181; http://dx.doi.org/10.17736/jowe.2015.mkr03
http://www.isope.org/publications/publications.htm

Wave Loads on a Point-Absorbing Wave Energy Device in Extreme Waves

Malin Göteman, Jens Engström, Mikael Eriksson and Mats Leijon
Department of Engineering Sciences, Uppsala University
Uppsala, Sweden

Martyn Hann, Edward Ransley and Deborah Greaves
School of Marine Science and Engineering, Plymouth University
Plymouth, UK

The survivability of a 1:20 scale point-absorbing Wave Energy Converter (WEC) model is considered in extreme wave tests with focused waves embedded in regular wave backgrounds and with time series of irregular waves. The wave heights were many times higher than the maximal stroke length of the device. Three different float geometries were used in the tests. The peak loads were measured and compared for extreme waves embedded in background waves with a range of periods and phase relations and with different values of Power Take-Off (PTO) damping.

INTRODUCTION

One of the most challenging problems for wave energy to be an economically viable energy source is to ensure reliable energy production and survivability in extreme weather conditions outside the normal operational wave climates.

Extreme waves are rare, but when they occur, they can lead to large structural damages to the offshore structure, which may be a platform, a ship, or a Wave Energy Converter (WEC). Extreme waves are surface gravity waves whose wave heights are much larger than expected for the sea state. They are characterized by a high crest between two deep troughs. Some studies indicate that extreme wave events are more common than previously thought (Dysthe et al., 2008) and their rate of occurrence is increasing (Ruggiero et al., 2010).

In ocean engineering, the impact of high and steep waves has been a subject of research for many decades (Molin, 1979; Mei, 1983; Lighthill, 1986; Eatock-Taylor and Hung, 1987). Different approaches to model the nonlinear behavior of steep waves include semi-empirical methods, nonlinear potential flow methods, full Computational Fluid Dynamics (CFD) methods, or combinations of these. However, CFD modelling is very computationally demanding, and all the numerical models still depend on physical experiments for validation. The impact of extreme waves is also highly dependent on the offshore structure in question.

Physical experiments of wave loads on truncated vertical cylinders were reported by Ransley et al. (2013), and the results were compared with numerical simulations with OpenFOAM (Open source Field Operation And Manipulation) and were in good agreement. For the point-absorbing wave energy converter Wavestar, physical tank tests were compared with computations of the Froude-Krylov forces and linear diffraction theory by Viuff et al. (2013).

In our study, we present experimental results of the forces of high, steep but nonbreaking waves on point-absorbing wave energy devices. The buoy is freely floating but attached to a linear power take-off (PTO) model with limited stroke length. Both focused waves embedded in regular wave backgrounds and irregular waves are studied, and the wave heights are several times the maximal stroke length of the device. In particular, this study analyses how the wave height of the individual waves affects the force peaks and the variability of the wave loads. In order to provide quick estimates and guidelines for developers of wave energy technologies, all set-up dimensions and the results will be presented in full-scale values.

Received April 8, 2015; revised manuscript received by the editors July 4, 2015. The original version was submitted directly to the Journal.
KEY WORDS: Wave energy, extreme waves, tank tests, power take-off (PTO) damping, maximum forces, survivability.

METHOD

Model

Through the use of Froude scaling, a 1:20 scale model was constructed on the basis of the point-absorbing wave energy converter developed at Uppsala University in Sweden. The dimensions of the model and the corresponding full-scale values are presented in Table 1 and can be seen in Fig. 1. The model consists of a float connected through a line and pulley system to a power take-off model situated on a gantry above the water level. The power take-off damping is modelled physically by a friction damping applied by adjustable Teflon blocks pressing against the translator that is moving vertically in the power take-off model.

The force that the friction break exerts on the moving translator is given in N units in Table 1. For a full-scale device, this corresponds to an electric damping in the generator at a constant translator speed. At the top end, the translator movement is damped by an end stop spring, which is also the case in the full-scale WEC, as can be seen in Fig. 1.

Several different documents with guidelines for WEC survivability experiments have been published. Holmes and Nielsen (2010) suggest that tests should be performed on both a small scale (1:100 up to 1:25) and a medium scale (1:25 up to 1:10). Here, a 1:20 scale was chosen as a compromise between a large enough scale to neglect friction and viscous effects and a small enough scale to be able to generate the correct amplitude of extreme waves in the wave tank.

Three different floats were used in the experiments: a cylinder float (CYL), a cylinder float with a moonpool (CM), and a cylinder float with a moonpool and additional water damping (CWD). The floats can be seen in Fig. 1. The float with a moonpool and no additional water damping is obtained by removing the top hat of the leftmost float in Fig. 1. The attachment point of the line to the power take-off is centered on the vertical axis for all the floats.

	1:1 Full-scale	1:20 Model
Buoy outer/inner radius of cylinder float with moonpool (CM) and cylinder float with moonpool and additional water damping (CWD)	2 m / 1.03 m	0.1 m / 0.052 m
Buoy radius of cylinder float (CYL)	1.7 m	0.085 m
Buoy draft of CM and CWD	0.94 m	0.047 m
Buoy draft of CYL	0.64 m	0.032 m
Translator stroke length	4.4 m	0.22 m
Buoy mass of CWD	8.6 tons	1.07 kg
Buoy mass of CM	7.2 tons	0.90 kg
Buoy mass of CYL	5.7 tons	0.72 m
Translator mass	6.24 tons	0.780 kg
Spring constant	776 kN/m	1.94 kN/m
PTO damping 1	~18 kN	~2.25 N
PTO damping 2	~59 kN	~7.38 N
PTO damping 3	~83 kN	~10.4 N
Water depth	50 m	2.5 m

Table 1 Dimensions of the model and the corresponding dimensions in the full-scale WEC. The PTO damping values are only approximate.

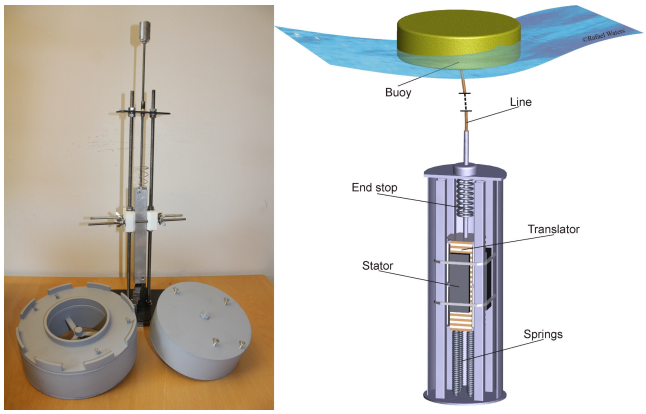

Fig. 1 The model used in the experiments and an illustration of the full-scale WEC. The full-scale PTO damping is electrical, whereas in the model it is asserted by friction brakes acting on the translator.

Extreme Wave Events

Extreme wave events are typically derived from site-specific historical wind and wave data, from which a return period of extreme waves can be statistically determined. A common return period for the survivability design of offshore structures is 100 years, but Coe and Neary (2014) suggest that an appropriate design criterion for WEC survivability is a return period of 50 years. For these experiments, an 80-year return period of the sea state at the Wave Hub site was chosen. The Wave Hub is located in southwest UK and constitutes one of the most energetic wave climate sites in Europe. On the 1:20 scale chosen for the experiments, the wave height of the 80-year return period of the extreme wave can be correctly reproduced in the wave basin through the use of the NewWave theory (Tromans et al., 1991), but the wave shape is slightly steeper.

All waves in the experiments are monodirectional, with negligible wave reflection from the sides of the wave basin. The extreme wave generation is described in more detail by Ransley et al. (2013).

Embedded Focused Waves. In the experiments, focused waves embedded in regular wave backgrounds were used. The focused waves were embedded into different phase positions within the regular wave. In total, 32 different embedded focused waves were used, divided into four sets with background periods of 10 s, 10.7 s, 12.7 s, and 13.7 s. The regular background wave height was 7.2 m for all the tests. Each of the four sets contained eight tests where the phase position for the embedding within the regular wave was $\pi(k-1)/4$, with $k = 1, \ldots, 8$. Here, the focused wave tests were labelled T_{jk}, where $j = 1, \ldots, 4$ represents the different background periods. The embedded focused waves were chosen so as to provide a more controlled experiment of extreme wave events and to study the wave load and the response of the float from the extreme wave in different background embeddings.

Irregular Waves. To provide more realistic conditions, experiments with time series of extreme irregular waves were also conducted. For offshore structures with constrained motions, such as a wave energy converter with a fixed mooring or a stroke length, nonextreme but high waves may also cause high forces and fatigue or damage to the structure, and a number of factors are likely to influence the device's response to the waves. Whereas the embedded focused wave tests provide information on the maximum force as a function of one incoming extreme wave with a determined wave height, the irregular wave tests measure the wave loads in a more unpredictable setting.

Two different time series of irregular waves were used, referred to as I_1 and I_2. Their spectra are generated through the use of the standard JONSWAP spectrum, and they differ in their significant wave heights ($H_s^{(1)} = 7.4$ m, $H_s^{(2)} = 7.2$ m) and in their energy periods ($T_e^{(1)} = 12.9$ s, $T_e^{(2)} = 11.7$ s). The time series of each irregular wave test is recorded for 67 minutes, which corresponds to 15 minutes on the 1:20 scale.

Experiments

The experiments were conducted at the Coastal Ocean And Sediment Transport (COAST) Laboratory at Plymouth University in the UK. The wave tank measures 35 m × 15.5 m, has a raiseable floor, and is equipped with 24 flap-type paddles. The surface elevation was measured with a set of calibrated resistive wave gauges. The force in the line was measured by a miniature low-profile load cell attached to the top of the translator and connected to the buoy through a nonelastic line. The mass of the load cell is 0.45 kg and is included in the full mass of the translator in Table 1.

The position of the buoy was measured with the optical Qualisys system, consisting of five cameras placed outside the basin and four infrared reflecting markers attached by rods to the buoy. The load cell and the motion capture system were synchronized and had a sampling frequency of 128 Hz.

RESULTS

Extreme Forces as Function of Wave Height

Embedded Focused Waves. For each of the 32 focused waves embedded in regular waves, the incoming waves were measured at a wave gauge close to the buoy. The wave peaks and troughs in each test were identified, as shown in Fig. 2. From Fig. 2, it is clear that the focused wave hits at 224 s and the remaining test cycle comprises regular waves of roughly the same height.

Each incoming wave was then correlated with the corresponding force measurement of the same test, as plotted in Fig. 3. More specifically, the maximal force in the time interval between two adjacent wave troughs was identified and is marked in Fig. 3 with

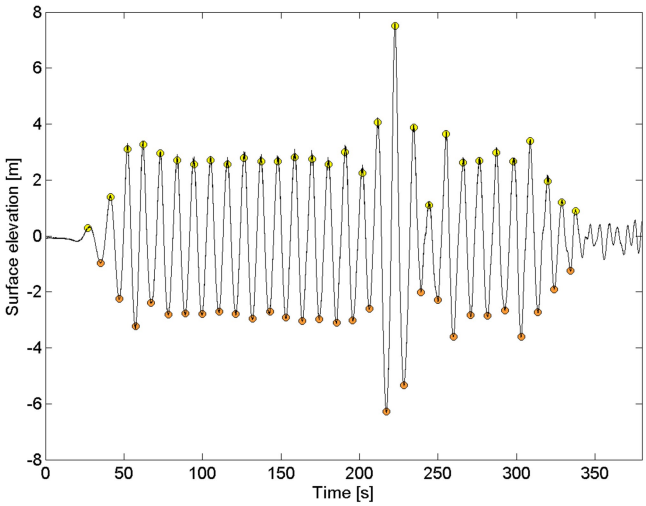

Fig. 2 Surface elevation measured at the float for the embedded focused wave test T_{11}, with corresponding force measurements shown in Fig. 3

a red asterisk. From Fig. 3, it is clear that the magnitude of the force peaks varies even in the regular wave background before the focused wave hits. For the test T_{11} plotted in Figs. 2 and 3, there are in total 29 wave troughs and 28 corresponding identified force peaks. This procedure was repeated in a systematical way for all 32 embedded focused wave tests. Depending on the background wave period, the amount of force peaks in each test ranges from 22 to 28. For each individual wave, the wave height was determined as the vertical distance from the preceding wave trough to the wave peak. Furthermore, negative large forces were measured when the translator hit the lower end stop at full speed. In a full-scale WEC, the motion will be damped. These negative peaks were omitted here.

All force peaks are plotted against the wave height of the corresponding wave in Fig. 4. Tests T_{jk} with $j = 1$ have a background period of 10.7 s and are plotted with asterisks (*); tests with $j = 2$ have a background period of 12.7 s and are plotted with points (.); tests with $j = 3$ have a background period of 13.7 s and are plotted with crosses ($\times$); and tests with $j = 4$ have a background period of 10.0 s and are plotted with pluses (+). The individual tests $k = 1, \ldots, 8$ are indicated by different colors, but will not be

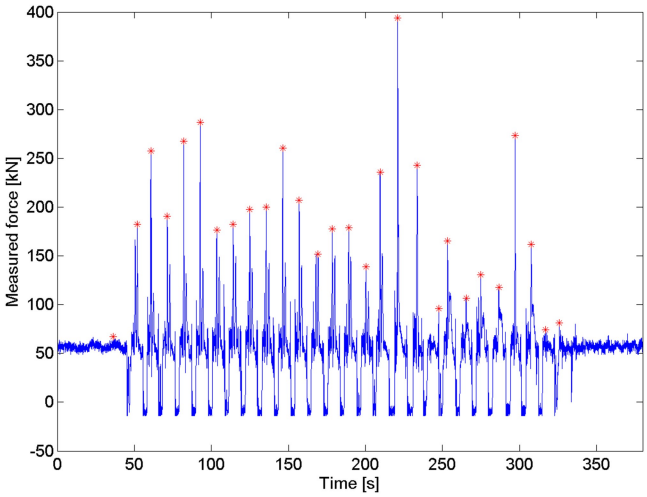

Fig. 3 Force measurements for the embedded focused wave test T_{11}, corresponding to the embedded focused wave data in Fig. 2

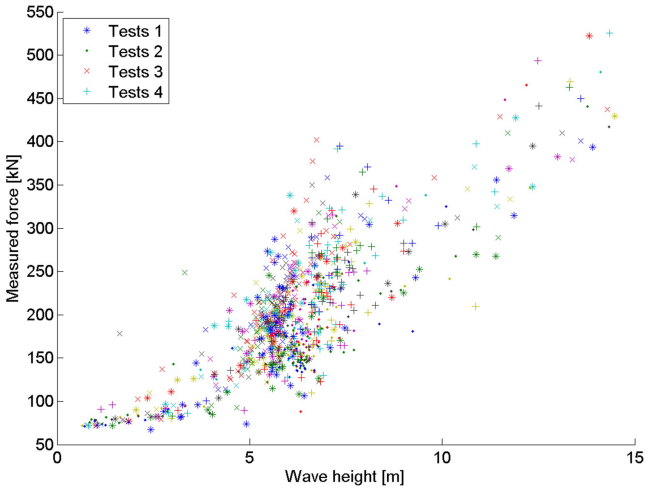

Fig. 4 Force peaks in all 32 tests with focused waves embedded in regular wave backgrounds. In each test, 22–28 force peaks were identified and are plotted. The accumulation of data points in the wave height range of 5–7 m corresponds to the regular wave background.

investigated in any detail here. All tests in Fig. 4 are performed for the cylinder float with a moonpool and water damping (CWD).

It is clear from Fig. 4 that the measured force follows a clear trend as a function of the wave height, with an accumulation of force peaks in the range of 100–350 kN for wave heights of 5–7 m, which corresponds to the regular wave background. The highest measured forces are obtained for the largest wave heights > 12 m. Still, despite the small variability in the wave height of the incoming waves, the variability in the measured force peaks is rather large. A corresponding scatter diagram in the case of nonzero PTO damping values is shown in Fig. 9.

Irregular Waves. The identification of the peaks and troughs of the irregular waves is not as straightforward as the identification of the peaks and troughs in the embedded focused wave tests discussed above. Figure 5 shows the surface elevation for a time period of 50 s. Unlike in the case of the regular waves in Fig. 2, we are not interested in all local wave peaks and troughs; rather, we are interested in only the waves with a large vertical trough-to-

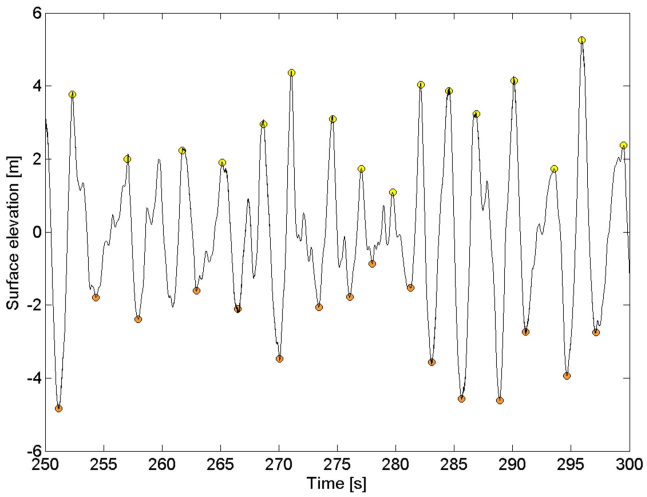

Fig. 5 Surface elevation for the irregular wave test I_2 as detected by a wave gauge in the direct vicinity of the cylinder float (CYL)

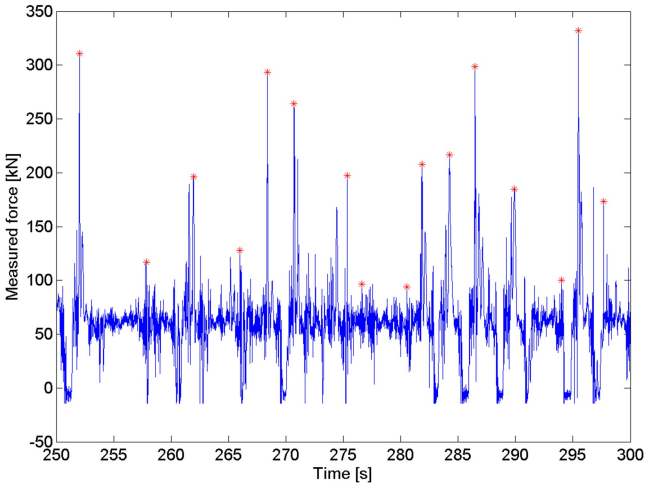

Fig. 6 Force measurements for the irregular wave test I_2 for the cylinder float (CYL), as well as the identified force corresponding to each individual wave in Fig. 5

peak distance. Hence, in the algorithm to determine the troughs and peaks, each peak is defined as the global maximum within 13.9 s from the previous peak, which implies that some local wave maximums and minimums were neglected, as can be seen in Fig. 5. The rest of the time spectrum for the irregular wave tests (67 minutes in total) looks similar, with almost all major troughs and peaks detected, but with some local extremes ignored. After the peaks and troughs in the irregular wave tests were identified, the corresponding maximum force between each pair of succeeding wave troughs was detected. The measured force together with the identified peak forces is shown in Fig 6, corresponding to the same test and time period shown in Fig. 5.

The force peaks are plotted against the wave height for each individual wave in Fig. 7, where the wave height is computed again as the vertical distance from the preceding trough to the wave peak. The irregular wave test I_1 for the cylinder float (CYL) is plotted with red asterisks, and the irregular wave test I_2 for the same float is plotted with black pluses. For both irregular wave tests, 268 force events were identified and plotted. The equivalent scatter

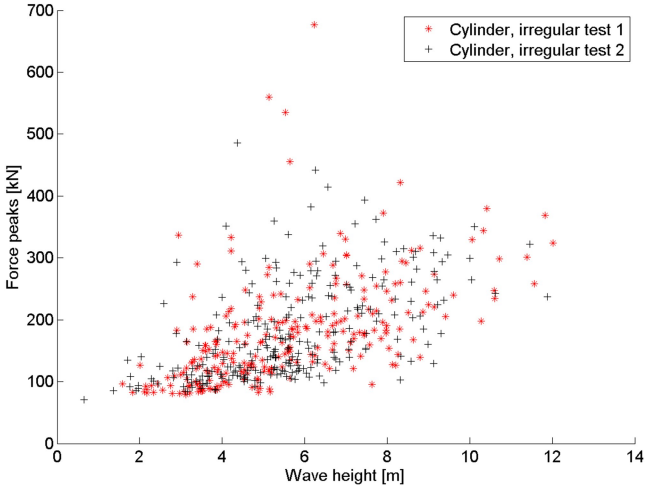

Fig. 7 Measured force peaks in irregular wave tests I_1 and I_2 for the cylinder float (CYL), plotted against the individual wave height of the incident wave

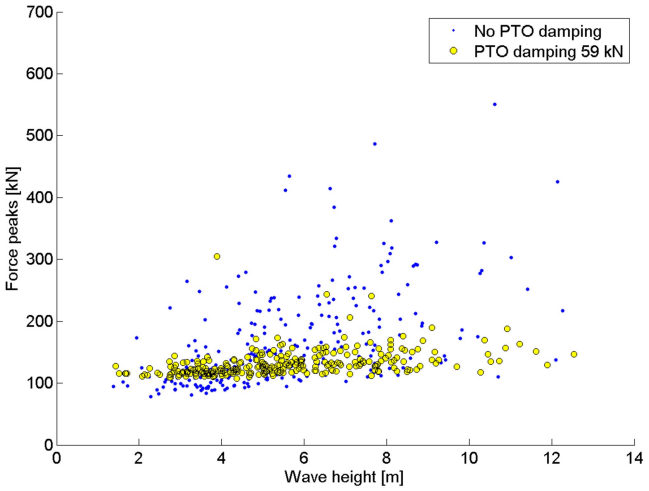

Fig. 8 Measured force peaks in irregular wave test I_1 for the cylinder float with moonpool (CM), plotted against the individual wave height of the incident wave

diagram of the cylinder float with a moonpool (CM) can be seen in Fig. 8 for both the case with and the case without PTO damping.

As can be seen in Fig. 7, there is a large variability of the detected maximum forces for the same wave height. A similar large variability of the total force as a function of the wave crest elevation was reported for extreme wave tests on vertical cylinders by Chaplin and Rainey (2012).

Extreme Forces as Function of PTO Damping

The WEC model in these experiments is equipped with a simple PTO damping consisting of Teflon blocks asserting friction brakes on the translator motion. All results presented in Figs. 2 to 7 refer to experiments performed with zero PTO damping. To investigate the influence of PTO damping, Fig. 8 compares irregular wave tests with and without damping and clearly shows that the PTO damping reduces the force measured in the line between the float and translator.

Similarly, in Fig. 9, one of the embedded focused wave tests, T_{12}, was plotted for the three cases with PTO damping: 18 kN,

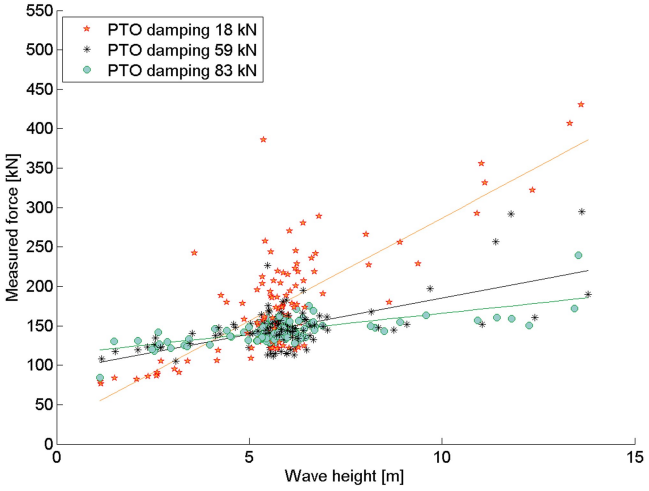

Fig. 9 Measured force peaks in the embedded focused wave test T_{12} for the CWD float with three different values of PTO damping. Linear trend lines were added for visibility. Compare Fig. 9 with the case without PTO damping in Fig. 4.

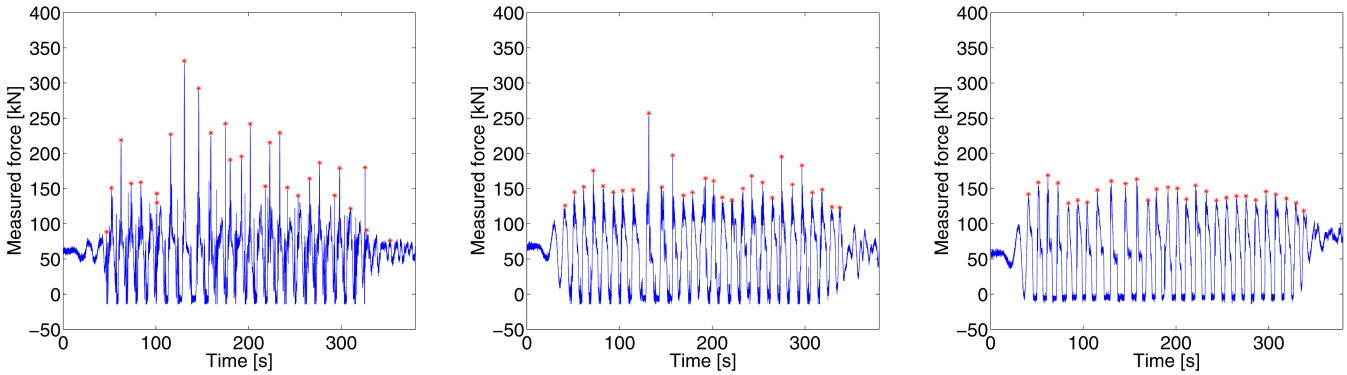

Fig. 10 Force measurements for the embedded focused wave test T_{12} with three different approximate values of the PTO damping: 18 kN (left), 59 kN (middle), and 83 kN (right)

59 kN, and 83 kN. When comparing Figs. 4 and 9, one observes that the damped cases (Fig. 9) display lower measured force peaks and the variability in the measured forces is reduced. The mean of the maximal force obtained in each of the 32 tests without PTO damping in Fig. 4 is 410 kN. The corresponding mean values for the maximal force obtained in each of the tests in Fig. 9 are 379 kN, 280 kN, and 187 kN, respectively, for the three increasing PTO damping values.

Finally, to complete the picture of the influence of the PTO damping, the corresponding time series of the measured force peaks in the three tests with PTO damping for the embedded focus wave test T_{12} are plotted in Fig. 10. In these tests, the embedded focused wave hits the float at $t = 134$ s. In the leftmost plot, a weak PTO damping of ~18 kN is used, and the variability in the force peaks is similar to that in the undamped test in Fig. 3. As the magnitude of the PTO damping increases to ~59 kN in the middle plot, the force peaks are effectively reduced, and in the overdamped system in the rightmost plot, there is no visible force peak due to the embedded focused wave.

Response of Different Floats in Extreme Waves

Three different floats were used in the tank tests. From a comparison of the irregular wave test I_1 without damping in Figs. 7 and 8, a slight tendency toward higher force peaks for the cylinder float (Fig. 7) than for the CM float (Fig. 8) can be perceived.

DISCUSSION

Both the embedded focused waves and the irregular waves examined in these experiments were nonbreaking and monodirectional with negligible reflections from the sides of the wave basin. It can be expected that the wave loads will decrease somewhat in omnidirectional waves (Parmeggiani et al., 2011).

The results in Figs. 2 to 7 show that the variability in the measured forces is very big. In the irregular wave tests, a certain amount of variability is expected, but the obtained variability in the measured force even in the regular wave background of the focused wave in Figs. 3 and 4 is somewhat surprising. From a comparison of the regular wave background in Fig. 2 with the corresponding force peaks in Fig. 3, the large variability can be quantified. The normalized standard deviation of the regular wave heights during the time interval of 50-190 s in Fig. 2 is only 0.08, but the normalized standard deviation of the corresponding force peaks during the same time interval in Fig. 3 is 0.2, i.e., 2.6 times higher. Furthermore, the variability in the measured forces in the irregular waves in Figs. 6 and 7 is larger than anticipated.

Not only the wave height but also the steepness of the individual waves will affect the motion of the float and the wave loads on the device. Although the wave loads are generally expected to grow with the wave height, there are possibly a number of local force maximums associated with certain wave periods and height combinations (Coe and Neary, 2014), which correspond to points of resonance, for instance.

In the regular wave backgrounds used for the embedded focused wave tests, four different values for the wave period were used, and the irregular wave tests contained a large spectrum of waves with different steepness. This may explain some of the variability in the force measurements between different tests and in the irregular tests, but it still does not explain the variability in the background regular waves (see Fig. 3).

Many factors may influence the wave loads on the device. For example, the position of the float at the instant the wave hits will possibly affect the measured forces. Even for the controlled experiments with regular waves, small deviations in the position due to the previous waves may influence the device's response to the waves and thereby affect the measured forces.

Despite the choice of the 1:20 scale, there is undoubtedly friction and viscosity present in the experiments, which adds to the uncertainties in the results. Another source of uncertainty in the experiments is the existence of the end stop spring. The scale model was designed with an end stop to resemble the full-scale wave energy device, where an end stop spring is used to damp the largest vertical motions of the translator and prevent damage to the generator hull or mooring lines during high waves. The magnitude of the spring force in the model was chosen so as to contract partly during the extreme wave tests but to never be fully contracted. The same spring was used throughout the experiments. In each wave cycle, the spring was retracted to its full length; hence a priori, the velocity of the float in waves of equal wave height should be exposed to the same force by the spring. Nevertheless, the spring was not completely fixed in a vertical position and could potentially have contracted differently in different wave cycles due to small differences in its position and the stiffness of the spring, which could possibly have influenced the measured forces. In future experiments, controlled tests with and without different end stop springs, which are possibly longer and with less stiffness, would be interesting.

Figures 8 to 10 show the measured force peaks in experiments with and without PTO damping. Figures 8 to 10 demonstrate how the force peaks are reduced when the PTO damping is increased. The variability in the measured force peaks is reduced when a PTO damping is applied, which can be seen in Figs. 9 and 10. The normalized variance of the peaks in the three tests with increasing

damping in Fig. 10 is 0.11, 0.031, and 0.0073 for 18 kN, 59 kN, and 83 kN, respectively.

Even in the case with PTO damping, there is a tendency toward an increased wave load with higher wave heights, as can be seen in Fig. 9, but the slope decreases and is almost flat for the overdamped system with the highest PTO damping.

CONCLUSIONS

A 1:20 scale model of a point-absorbing wave energy converter was subjected to extreme wave tests using both focused waves embedded in a regular wave background and time series of irregular waves. The force in the line connecting the buoy and generator was measured, and the force peaks were matched with the corresponding incident waves. This enabled an analysis of the force peaks as a function of the individual wave height of the incident extreme waves.

Our results show that the variability in the measured force peaks is large, even in the regular background waves with roughly the same wave heights. In the irregular wave tests, the scattering among the force peaks is even larger. A PTO damping applied to the model reduces not only the average magnitude but also the variability in the measured peak forces.

ACKNOWLEDGEMENTS

This research is supported by StandUp for Energy, Uppsala University, Carl Tryggers Stiftelse, the Swedish Energy Agency, the Bengt Ingeströms scholarship fund, the Wallenius Foundation, and Miljöfonden.

REFERENCES

Chaplin, JR, and Rainey, RCT (2012). "Long-duration Experiments in Irregular Waves, to Determine 10,000-year Wave Loads on a 3.5 m Diameter Vertical Cylinder," In: *Proc 27th Int Workshop Water Waves Floating Bodies (IWWWFB)*, HB Bingham, RW Read and TB Christiansen (Eds), Copenhagen, Denmark.

Coe, RG, and Neary, VS (2014). "Review of Methods for Modeling Wave Energy Converter Survival in Extreme Sea States," *Proc 2nd Mar Energy Technol Symp (METS)*, Seattle, WA, USA. http://hdl.handle.net/10919/49221.

Dysthe, K, Krogstad, H, and Müller, P (2008). "Oceanic Rogue Waves," *Annu Rev Fluid Mech*, 40, 287–310. http://dx.doi.org/10.1146/annurev.fluid.40.111406.102203.

Eatock-Taylor, R, and Hung, S (1987). "Second Order Diffraction Forces on a Vertical Cylinder in Regular Waves," *Appl Ocean Res*, 9(1), 19–30. http://dx.doi.org/10.1016/0141-1187(87)90028-9.

Holmes, B, and Nielsen, K (2010). *Guidelines for the Development & Testing of Wave Energy Systems*, OES-IA Tech Report T02-2.1, Ocean Energy Systems (OES).

Lighthill, J (1986). "Fundamentals Concerning Wave Loading on Offshore Structures," *J Fluid Mech*, 173, 667–681. http://dx.doi.org/10.1017/S0022112086001313.

Mei, C (1983). *The Applied Dynamics of Ocean Surface Waves*, Wiley-Interscience, 740 pp.

Molin, B (1979). "Second-order Diffraction Loads Upon Three-dimensional Bodies," *Appl Ocean Res*, 1(4), 197–202. http://dx.doi.org/10.1016/0141-1187(79)90027-0.

Parmeggiani, S, Kofoed, J, and Friis-Madsen, E (2011). "Extreme Loads on the Mooring Lines and Survivability Mode for the Wave Dragon Wave Energy Converter," *Proc World Renewable Congress*, Linköping, Sweden, 2159–2166.

Ransley, E, Hann, M, Greaves, D, Raby, A, and Simmonds, D (2013). "Numerical and Physical Modelling of Extreme Wave Impacts on a Fixed Truncated Circular Cylinder," In: *Proc 10th Eur Wave Tidal Energy Conf (EWTEC)*, Aalborg, Denmark.

Ruggiero, P, Komar, P, and Allan, J (2010). "Increasing Wave Heights and Extreme Value Projections: The Wave Climate of the U.S. Pacific Northwest," *Coastal Eng*, 57(5), 539–552. http://dx.doi.org/10.1016/j.coastaleng.2009.12.005.

Tromans, P, Anaturk, A, and Hagemeier, P (1991). "A New Model for the Kinematics of Large Ocean Waves—Application as a Design Wave," *Proc 1st Int Offshore Polar Eng Conf,* Edinburgh, Scotland, ISOPE, 3, 64–71.

Viuff, T, Andersen, M, Kramer, M, and Jakobsen, M (2013). "Excitation Forces on Point Absorbers Exposed to High Order Non-linear Waves," In: *Proc 10th Eur Wave Tidal Energy Conf (EWTEC)*, Aalborg, Denmark.